Zhao *et al. Biochar* (2026) 8:145
https://doi.org/10.1007/s42773-026-00662-4

Biochar

ORIGINAL RESEARCH Open Access

Valorization of biogas digestate through hydrothermal humification for nitrogen-enriched artificial humic acid production

Yanan Zhao[1,2], Ziyun Liu[1,2*†], Zonglu Yao[1,2], Dan Wang[1,2], Jinting Su[1,2], Jihua Yang[3], Lili Huo[1,2], Jixiu Jia[1,2], Hugang Li[4] and Lixin Zhao[1,2*†]

Abstract

Biogas digestate (BD), a nutrient-rich and low-cost carbon source, can be converted into artificial humic acid (AHA) through hydrothermal humification (HTH). However, the process is often constrained by low efficiency and inconsistent product quality. In this study, the effects of different reaction media, including biogas slurry (BS) and deionized water, on the properties of AHA derived from BD at various temperatures (180–260 °C) were investigated. The results showed that BS addition increased both AHA yield and nitrogen content, with a maximum AHA selectivity of 40.16% in the hydrochar at 220 °C. FT-ICR-MS, 3D-EEM, and solid-state ^{13}C NMR analyses indicated that lignin in BD was the main precursor for aromatic AHA synthesis in the deionized water system. When BS was introduced into the HTH process, lignin depolymerization and nitrogen-involving Maillard reactions were likely enhanced, resulting in greater nitrogen incorporation into AHA, with a maximum of 26.02 mg N retained in AHA at 220 °C. This enhanced nitrogen retention was associated with the formation of reactive intermediates and subsequent incorporation of nitrogen into more stable heterocyclic structures. This study provides a sustainable pathway for the efficient conversion of biogas plant residues into nutrient- and humic-rich products with potential as soil amendments.

Highlights

- BD was efficiently converted into AHA through HTH.
- BS served as a reactive medium and nitrogen source to enhance AHA production.
- Maillard-type reactions promoted nitrogen-rich AHA formation in the BS system.

Keywords Hydrothermal humification, Biogas digestate, Reaction medium, Nitrogen-rich artificial humic acid, Hydrochar

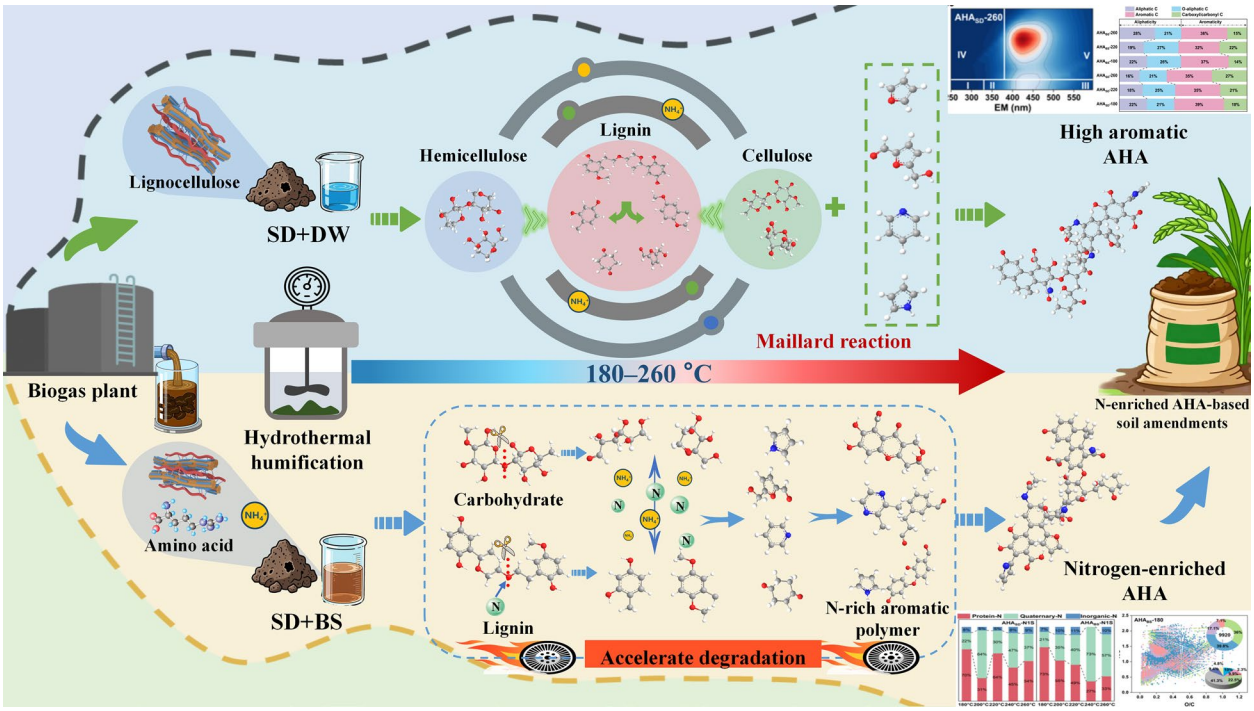
†Ziyun Liu and Lixin Zhao have contributed equally to this article and are joint corresponding authors.

*Correspondence:
Ziyun Liu
liuziyun@caas.cn
Lixin Zhao
zhaolixincaae@163.com
Full list of author information is available at the end of the article

© The Author(s) 2026. **Open Access** This article is licensed under a Creative Commons Attribution 4.0 International License, which permits use, sharing, adaptation, distribution and reproduction in any medium or format, as long as you give appropriate credit to the original author(s) and the source, provide a link to the Creative Commons licence, and indicate if changes were made. The images or other third party material in this article are included in the article's Creative Commons licence, unless indicated otherwise in a credit line to the material. If material is not included in the article's Creative Commons licence and your intended use is not permitted by statutory regulation or exceeds the permitted use, you will need to obtain permission directly from the copyright holder. To view a copy of this licence, visit http://creativecommons.org/licenses/by/4.0/.

Springer

Graphical Abstract



1 Introduction

Driven by the global transition toward clean energy and the development of a circular economy, large-scale anaerobic digestion technology has become increasingly important for waste valorization and renewable energy recovery (Ahmad et al. 2018; Devi and Eskicioglu 2024). However, this process generates substantial quantities of biogas digestate (BD) as a byproduct, with China alone generating over 400 million tons annually (Song et al. 2025). The high moisture content (typically >80%), complex composition, and potential environmental risks of BD limit its efficient utilization (Mikusińska et al. 2025; Kim et al. 2020).

Hydrothermal humification (HTH) has recently emerged as a promising strategy for converting wet organic wastes into artificial humic acid (AHA), an active humic-like component with potential value for soil amendment and nutrient-return applications, under subcritical conditions (150–350 °C, 5–250 bar) without energy-intensive drying or additional water input (Basar et al. 2021; Liu et al. 2024; Zhu et al. 2024). It should be noted that AHA is operationally defined as a humic acid-like substance rather than an exact structural replica of naturally occurring humic acid. Although they share key physicochemical features, they can differ in molecular structure due to the abiotic and short-timescale synthesis pathway. This target product differs substantially from the highly carbonized, humin-like hydrochar typically produced by conventional hydrothermal carbonization (HTC). Although HTH and HTC share similar subcritical reaction conditions, HTC mainly generates highly condensed carbonaceous materials that are used as solid fuels or catalyst carriers (Cao et al. 2019; Xu et al. 2019). In contrast, HTH aims to direct biomass-derived intermediates toward the formation of AHA with humic acid-like structural features, including aromatic carbon domains and abundant oxygen-containing functional groups, rather than extensive carbonization, by regulating alkaline catalysts, nitrogen-containing additives, and temperature–time conditions (Wang et al. 2025; Liu et al. 2024; Shao et al. 2023a, b). Due to its unique aromatic structure and abundant oxygen-containing functional groups, AHA plays a crucial role in agriculture and environmental remediation, including soil carbon sequestration, microbial activity stimulation, nutrient and moisture retention, and soil structure improvement (Deng et al. 2023; Guo et al. 2019; Lehmann et al. 2020). However, the efficient formation of AHA during the HTH process remains challenging, as the reaction

mechanisms and influencing factors governing humification are not yet fully understood.

Nitrogen incorporation can enrich AHA with nitrogen-containing functional groups and increase its nitrogen content. During HTH, these nitrogen-containing substances can react with carbonyl compounds generated from carbohydrate degradation through the Maillard reaction, which serves as a key pathway for the formation of AHA macromolecules (Zhou et al. 2022). Chen et al. investigated the HTH of food waste and demonstrated that AHA formation was enhanced by the Maillard reaction between amino acids and glucose, achieving an optimal yield of 43.5% (Chen et al. 2022). Similarly, Wang et al. treated agricultural waste with organic and inorganic nitrogen-containing additives to produce nitrogen-enriched AHA with a N content increase of approximately 30.44% (Wang et al. 2025). When lignin reacts with nitrogen-containing substances, the resulting nitrogen-rich AHA typically shows excellent slow-release behavior, making it an effective controlled-release nitrogen fertilizer (Lu et al. 2022).

BD retains most of the original feedstock mass (70–90%), carbon content and energy (approximately 60%), and is rich in AHA precursors such as cellulose and lignin (Zhang et al. 2018). The liquid fraction of BD, referred to as biogas slurry (BS), contains abundant nitrogenous compounds derived from protein degradation (e.g., ammonium ions, amino acids, and peptides) (Ke et al. 2022; Liu et al. 2025). The abundant ammonia nitrogen and organic acids in BS, functioning as catalysts or reactive intermediates during hydrothermal processes, enhance the yield and nitrogen content of hydrochar (Wang et al. 2024), while also potentially contributing to AHA formation. Unlike many previously reported HTH systems that rely on externally added alkali or nitrogen sources (Wang et al. 2025; Shao et al. 2023a, b), BS inherently provides a mildly alkaline reaction environment (pH ≈ 8.0) and abundant nitrogen-containing components, such as ammonium nitrogen and amino acids (Song et al. 2025), reducing the need for external chemical inputs. Moreover, BD and BS are generated together in large quantities at biogas plants, and their combined HTH treatment therefore provides a practical and potentially scalable pathway for integrated waste management and value-added product recovery. In addition, reaction temperature is a key parameter influencing AHA structure, as elevated temperatures promote aromatization and polycondensation reactions (Shao et al. 2023a, b; Liu et al. 2024). Nevertheless, the mechanisms of BS-enhanced AHA formation during HTH of BD remain inadequately elucidated. In particular, the kinetic behavior at different temperatures and the synergistic regulation of key reaction pathways still lack systematic investigation.

Herein, this study aimed to investigate the effects of different hydrothermal media (BS and deionized water) on the yield and properties of AHA during the HTH process of BD. Briefly, the main objectives of this study were to: (1) investigate the effects of temperature and reaction medium on the yield, selectivity, and elemental composition of AHA; (2) elucidate the role of BS as a reaction medium in governing the structural evolution, nitrogen fixation, and reaction pathways of AHA; and (3) reveal the mechanisms underlying temperature- and reaction medium-driven evolution of functional groups and chemical structures in AHA. This work provides a theoretical foundation for optimizing the HTH process of BD and offers new insights into the sustainable production of nutrient-rich AHA-based soil amendments.

2 Materials and methods

2.1 Materials and reagents

BD samples were obtained from a large-scale anaerobic digestion plant located in Hebei Province, China. The plant primarily treats cattle manure and corn straw as feedstocks. The BD was separated into solid digestate (SD) and liquid BS using a screw press separator. The SD was oven-dried at 105 °C for 12 h, ground into powder and sieved through a 60-mesh screen prior to subsequent experiments. The BS was centrifuged at 3000 rpm for 15 min to remove suspended solids. The resulting supernatant was transferred into polyethylene bottles and stored at − 18 °C until analysis. All chemical reagents used in this study were of analytical grade and purchased from Yuanye Biotechnology Co. Ltd. (Beijing, China). The basic physicochemical properties of the BD are presented in Table 1.

2.2 HTH process and AHA extraction

Briefly, 6.0 g of SD was mixed with 54 mL of deionized water or BS in a 100 mL stainless steel Parr autoclave reactor (Model 4545, Parr Instrument Co., USA). The reactor was heated to the target temperatures (180, 200, 220, 240, and 260 °C) at a rate of 15 °C min^{-1} under continuous stirring and maintained at the designed temperature for 2 h, with an estimated pressure range of approximately 1.0–4.7 MPa based on the saturated vapor pressure of water. Subsequently, the reactor was cooled to room temperature. The products were separated into solid hydrochar and an aqueous phase via vacuum filtration. The hydrochar was thoroughly washed with deionized water and oven-dried at 105 °C for 24 h. The aqueous phase was filtered through a 0.45 μm membrane, transferred to glass bottles, and stored at −18 °C for subsequent analyses. The solid and liquid products

Table 1 Basic physicochemical properties of biogas digestate

SD (wt.%, dry basis)				BS	
Proximate analysis		**Component analysis**		**Property**	**Value**
Ash	24.96±0.23	Cellulose	19.53±0.17	pH	7.90±0.10
Volatile	59.50±0.10	Hemicellulose	10.27±0.13	TOC (g L^{-1})	1.79±0.02
Fixed carbon	8.57±0.30	Lignin	26.10±0.10	NH_4^+-N (g L^{-1})	1.16±0.01
		Crude protein	10.20±0.10	TN (g L^{-1})	1.17±0.03
		Crude fat	0.03±0.01		

were denoted as HC_R-T and AP_R-T, respectively, where R represents the feedstock and T indicates the HTH reaction temperature.

AHA was extracted from hydrochar following a modified International Humic Substances Society (IHSS) standard procedure (Hayes and Swift 2020). Briefly, 0.5 g of hydrochar was extracted with 40 mL of 0.1 M $Na_4P_2O_7$ and 0.1 M NaOH at 90 °C for 1 h. The mixture was centrifuged (8000 rpm, 5 min), and the extraction was repeated until the supernatant became colorless. The collected supernatants were combined and acidified to pH 1–2 with 6 M HCl, followed by standing for 12 h. The precipitate was recovered by centrifugation (10,000 rpm, 5 min), washed with deionized water, and dried at 105 °C for 24 h. All hydrothermal and AHA extraction experiments were performed independently in triplicate for each condition, and statistical significance analysis was conducted. A schematic illustration of the experimental workflow is provided in Fig. S1 of the Supporting Information.

2.3 Analytical methods

Proximate analysis was conducted according to standard procedures. Ash content was determined by combusting the sample in a muffle furnace at 550 °C for 5 h in air. Volatile matter content was measured by heating the dried sample at 900 ± 10 °C for 7 min in air using a covered crucible. Fixed carbon content was calculated by difference. All values are reported on a dry basis, and all measurements were performed in triplicate (Marzban et al. 2024). The elemental composition (C, H, N, and S) of hydrochar and AHA samples was analyzed using an elemental analyzer (Elementar UNICUBE, Germany). The oxygen (O) content was determined by difference.

Surface functional groups of AHA were characterized using Fourier transform infrared spectroscopy (FTIR) and X-ray photoelectron spectroscopy (XPS). For FTIR analysis, freeze-dried AHA (2 mg) was homogenized with potassium bromide (KBr, IR grade; 100 mg) and pressed into translucent pellets. Spectra were recorded using a Fourier transform infrared spectrometer (Nicolet iS5, Thermo Fisher, USA) at a resolution of 8 cm^{-1} over the 4000–400 cm^{-1} range, followed by two-dimensional correlation spectroscopy (2D-COS) analysis using 2Dshige software (Kwansei Gakuin University, Japan) (Gao et al. 2022). XPS spectra of AHA were obtained using a Thermo Fisher Scientific K-Alpha XPS Spectrometer equipped with a monochromatic Al Kα X-ray source (spot size, 400 μm; K-Alpha, Thermo Fisher, USA). High-resolution spectra of the C 1 s, O 1 s, and N 1 s core levels were recorded at a pass energy of 100 eV, and spectral deconvolution was performed using XPSPEAK software (Gao et al. 2022).

The fluorescence characteristics of AHA were analyzed using three-dimensional excitation-emission matrix (3D-EEM) spectroscopy (Cary Eclipse, Agilent, USA). Emission spectra were collected over a wavelength range of 240–600 nm, with excitation wavelengths ranging from 220 to 400 nm at 10 nm intervals and a scanning speed of 600 nm min^{-1} (Su et al. 2024). Solid-state ^{13}C nuclear magnetic resonance (NMR) spectra of AHA were measured using a Bruker Avance Neo 400WB spectrometer (Germany), operating at a resonance frequency of 150 MHz with a 3.2 mm rotor spinning at 12 kHz (Shao et al. 2023a, b). The molecular composition of dissolved organic matter (DOM) in AHA samples was characterized using Fourier transform ion cyclotron resonance mass spectrometry (FT-ICR-MS; SolariX, Bruker, USA). Prior to analysis, AHA samples were desalted by solid-phase extraction (SPE, 500 mg 6 mL^{-1} Bond Elut PPL cartridges, Agilent, USA). Briefly, the filtered sample was extracted through sequential acidification (pH 2.0), column activation, sample loading, rinsing, and methanol elution after N_2 drying. The extract was reconstituted in methanol/water (1:1, v/v) for FT-ICR-MS analysis. The detailed procedure is described in the Supplementary Materials. To evaluate molecular aromaticity, the degree of unsaturation or C=C double-bond density was first assessed. The sum of rings and double bonds in each molecule was expressed as the double bond equivalent (DBE), and was calculated as follows (Hu et al. 2025):

$$DBE = 1 + 0.5 \times (2C - H + N + P) \quad (1)$$

The modified aromaticity index (AI_{mod}) was used to distinguish aromatic cyclic compounds ($0.5 < AI_{mod} < 0.67$), polycyclic aromatic compounds ($AI_{mod} \geq 0.67$), and non-aromatic compounds ($AI_{mod} \leq 0.5$), and was calculated as follows:

$$AI_{mod} = \frac{1 + C - 0.5 \times O - S - 0.5 \times (N + P + H)}{C - 0.5 \times O - N - S - P} \quad (2)$$

where C, O, N, H, S, and P represent the numbers of carbon, oxygen, nitrogen, hydrogen, sulfur, and phosphorus atoms, respectively. AM_W, $(O/C)_W$, $(H/C)_W$ and DBE_W represent the intensity-weighted average molecular weight, O/C ratio, H/C ratio, and DBE, respectively, and are listed in Table S7.

To further elucidate the composition of the aqueous phase, gas chromatography–mass spectrometry (GC–MS; Agilent 7890B-5977A, USA) equipped with a DB-5 capillary column (30 m × 0.25 mm × 0.25 μm) and a mass selective detector (MSD) was used to analyze the molecular composition of organic compounds in the aqueous phase. Detailed operation conditions and data analysis methods followed the procedures reported previously (Liu et al. 2024). The total organic carbon (TOC) content of the aqueous phase was measured using a TOC-VCPN analyzer (Shimadzu, Japan). Total nitrogen (TN), ammonia nitrogen (NH_4^+–N), and nitrate nitrogen (NO_3^+–N) in the aqueous phase were measured according to standard methods (Wang et al. 2025).

2.4 Calculation methods

The yield and selectivity of AHA were calculated using Eqs. (3) and (4).

$$Y_{AHA} = \frac{M_{AHA}}{M_F} \times 100\% \quad (3)$$

$$S_{AHA} = \frac{M_{AHA}}{M_{HC}} \times 100\% \quad (4)$$

where, Y_{AHA} and S_{AHA} represent the yield and selectivity of AHA, respectively; M_{AHA}, M_F and M_{HC} denote the masses (g) of AHA, feedstock, and hydrochar, respectively.

3 Results and discussion

3.1 Variations of AHA yield and selectivity

Figure 1a presents the variations in hydrochar yield, as well as the selectivity and yield of AHA, under different reaction medium and temperature conditions. As the reaction temperature increased from 180 °C to 260 °C, the yield of HC_{SD} decreased by 32.62%, while that of HC_{BS} declined by 25.86%. This temperature-dependent reduction in hydrochar yield could be associated with enhanced conversion of insoluble digestate components into soluble low-molecular-weight intermediates, which subsequently entered the aqueous phase at elevated temperatures (Li and Cai 2022). A notable enhancement in hydrochar yield was observed when BS was used. This increase may be related to the high amino acid and ammonium contents in BS, which could participate in Maillard-type reactions with reducing sugars and promote the formation of nitrogen-containing products that may subsequently be incorporated into the hydrochar. This is also consistent with the observed changes in liquid-phase composition (Song et al. 2025).

The AHA selectivity exhibited distinct temperature-dependent trends depending on the reaction medium. AHA_{SD} selectivity initially decreased and then increased with rising temperature, which could be attributed to the rapid hydrolysis of readily degradable organic components (e.g., proteins, hemicellulose, and partial amorphous cellulose) at 180–220 °C, generating soluble intermediates such as sugars, amino acids, and organic acids that could partition into the aqueous phase. At higher temperatures, these intermediates may further participate in reactions such as Maillard-type reactions and polyphenol coupling, favoring the formation of more aromatic and polymerized AHA through polycondensation pathways (Fan et al. 2018). In contrast, AHA_{BS} selectivity reached a maximum value of 40.16% at 220 °C, followed by a gradual decrease at higher temperatures. This decline could be attributable to several concurrent processes: (a) pre-formed AHA may undergo further thermal depolymerization into soluble products; (b) increasing hydrothermal severity may favor excessive carbonization and condensation of organic precursors into hydrochar rather than AHA (Liu et al. 2024); and (c) nitrogen-rich substances derived from BS could undergo greater decomposition at elevated temperatures, thereby limiting their contribution to AHA formation (Zhang et al. 2022). These are consistent with the FT-ICR-MS results, which revealed temperature-dependent shifts in the molecular composition of the liquid-phase products. In conclusion, temperature and reaction medium appeared to exert synergistic effects on the selectivity and yield of AHA during the HTH process, highlighting their importance in regulating product quality and conversion efficiency.

3.2 Elemental composition of hydrochar and AHA

The elemental compositions of hydrochar and AHA are shown in Fig. 1b. For AHA_{SD}, the C content exhibited temperature-dependent fluctuations, reaching a maximum at 220 °C. In contrast, the C content of AHA_{BS} displayed an initial decrease within the 180–240 °C range, followed by a notable increase at 260 °C, which could

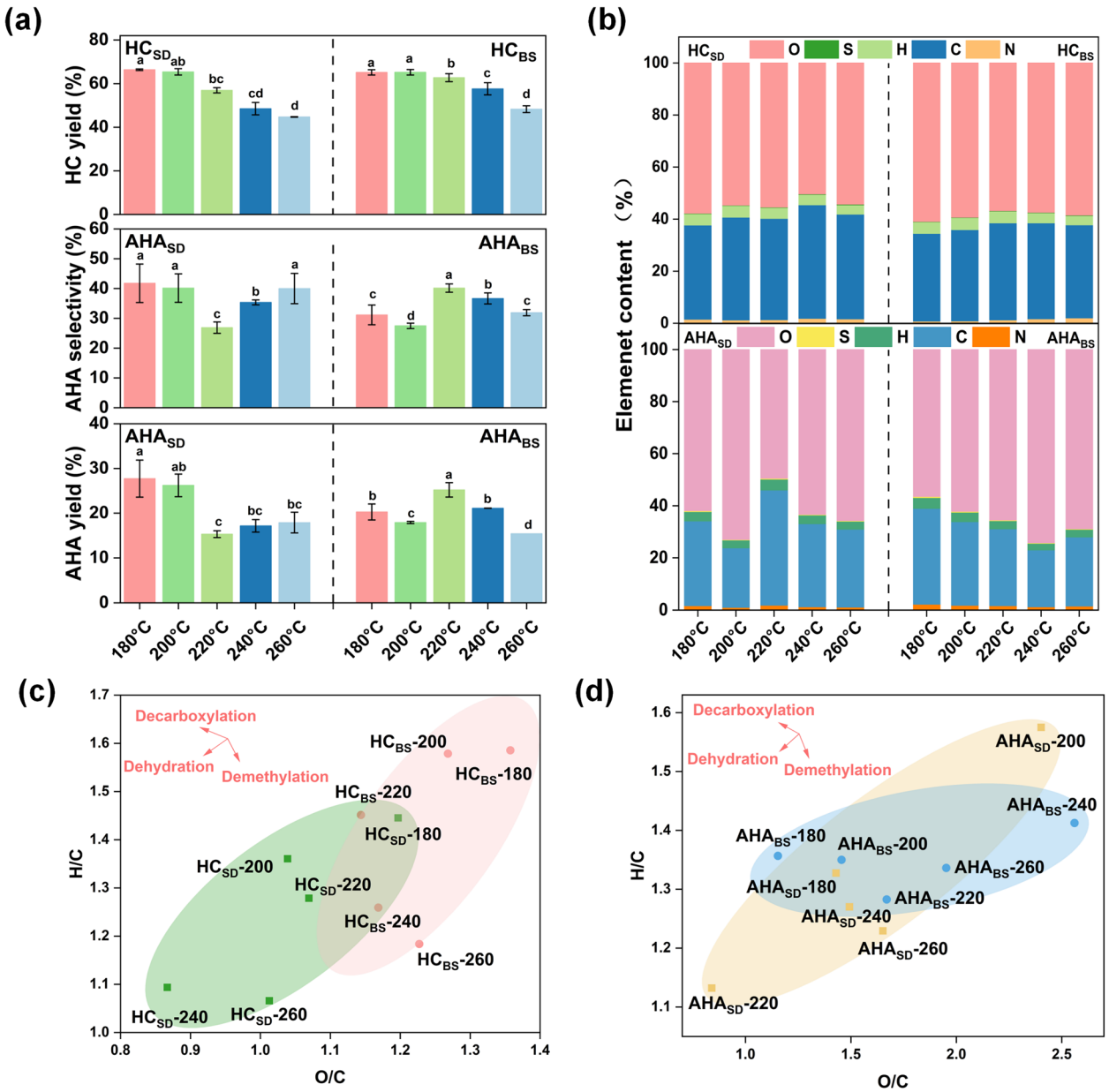


Fig. 1 Effect of temperature and reaction medium on BD humification during the HTH process: **a** hydrochar and AHA yields and AHA selectivity; **b** elemental compositions of hydrochar and AHA; and H/C and O/C molar ratios of **c** hydrochar and **d** AHA under different temperatures and reaction media

be related to the complex composition of BS that contains abundant ammonia nitrogen, inorganic salts, and organic acids. This discrepancy could also be associated with the effects of these diverse components in BS on the hydrolysis and transformation of lignin and cellulose (such as amino acids, ammonium nitrogen and organic acids) in BS (Liu et al. 2019; Song et al. 2025), which could enhance solubilization and secondary carbonization at elevated temperature. This is consistent with the selectivity behavior of AHA_{BS}. Notably, the nitrogen content in AHA_{BS} was significantly higher than that in AHA_{SD}.

The H/C and O/C molar ratios of hydrochar and AHA reflect the humification degree and structural characteristics (Fig. 1c and 1d). Generally, lower H/C ratios indicate a higher degree of aromatic condensation, while higher O/C ratios suggest greater oxidation and enrichment of oxygen-containing functional

groups (e.g., carboxyl and phenolic hydroxyl groups) (Chen et al. 2022). For hydrochar, both H/C and O/C ratios were lower in HC_{SD} than in HC_{BS} and decreased significantly with rising temperature. This suggests that decarboxylation and dehydration were enhanced during HTH, which could contribute to a more condensed aromatic structure in HC_{SD}. For AHA, the lowest O/C and H/C ratios were observed in AHA_{SD} at 220 °C, indicating a high degree of aromatization that could be associated with enhanced dehydration and decarboxylation. In contrast, AHA_{BS} maintained relatively higher O/C ratios up to 240 °C, suggesting better preservation of oxygen-containing functional groups. This phenomenon could be associated with BS-mediated hydrolysis and the formation of oxygen-rich intermediates (e.g., carboxylic acids and polyhydroxy compounds) that could subsequently contribute to AHA formation. Compared with AHA_{SD}, the N content increased by 80.95% in AHA_{BS}−200, suggesting that nitrogen-containing compounds in BS could participate in AHA formation. A C/N ratio exceeding 24:1 can result in temporary nitrogen deficiency (Celletti et al. 2021). The C/N ratios of AHA_{BS} were all below the critical threshold of 24:1 and significantly lower than those of AHA_{SD} (Table S3), suggesting that AHA_{BS} could have greater potential as a nitrogen-rich soil amendment. Based on the nitrogen mass balance analysis (Table S4), adding BS increased the total nitrogen input from 97.92 mg to 161.10 mg. After the HTH reaction, the nitrogen amounts in AHA and hydrochar generally increased, particularly at 220–260 °C. For example, at 220 °C, the nitrogen amount in AHA increased from 17.72 mg to 26.02 mg, while that in hydrochar increased slightly from 45.78 mg to 47.53 mg, supporting greater retention of BS-derived nitrogen in the AHA fraction.

3.3 Physicochemical characterization of AHA

3.3.1 Chemical structure

2D-COS based on FTIR was employed to investigate the dynamic evolution of functional groups in AHA with increasing temperature (180–260 °C). Figure 2a presents the synchronous and asynchronous maps of AHA_{SD} in the 800–1800 cm^{-1} region. The synchronous map displayed six auto-peaks along the diagonal, corresponding to trans-alkene C–H bending (975 cm^{-1}), C–O–C stretching (1080 cm^{-1}), aliphatic C–H deformation and/or symmetric stretching of carboxylate groups (–COO^-, 1442 cm^{-1}), amide II of proteins and/or aromatic C–N stretching in lignin-derived structures (1513 cm^{-1}), aromatic C=C stretching (1600 cm^{-1}), and C=O stretching of esters, acids, and ketones (1700 cm^{-1}) (**Fig. S2**) (Cai et al. 2023). The strong positive auto-peak observed at 975 cm^{-1} indicates a pronounced temperature-dependent variation in the corresponding trans-alkene C–H signal.

According to the asynchronous map, the sequential changes in functional groups with increasing HTH temperature followed the order 1442 → 1513 → 1600 → 1700 → 1080 → 975. This sequence suggests that carboxylate- and/or aliphatic C–H-related structures responded first during the lower-temperature stage, followed by changes in amide II and/or aromatic C–N structures. At the intermediate-temperature stage, the response of aromatic C=C groups became more pronounced, which could be associated with the progressive formation or enrichment of aromatic structures. With further temperature elevation, changes in the C=O and C–O–C bands became evident, which could reflect enhanced condensation and possible esterification/etherification processes. The late response of the 975 cm^{-1} band could be associated with further changes in trans-alkene-related structures and their possible transformation toward more conjugated structures (Daer et al. 2024; Zhang et al. 2022).

Compared with AHA_{SD}, the AHA_{BS} exhibited a greater number of auto-peaks, higher peak intensities, and the emergence of strong positive bands at 1740 cm^{-1} (ester C=O) and 1680 cm^{-1} (conjugated carbonyl C=O) (Fig. 2b), suggesting a higher degree of oxidation and greater enrichment of oxygen-rich functional groups, such as carboxyl and ester moieties. In AHA_{BS}, structures of oxygen-containing compounds appeared to respond earlier and showed changes concurrent with those of aromatic structures. This phenomenon could be associated with the formation and transformation of reactive oxygen-containing intermediates under BS conditions, which could facilitate subsequent condensation and structural diversification of degradation products, thereby contributing to a greater diversity of AHA functional groups (Zhang et al. 2022).

3.3.2 Surface composition

The surface chemical composition of AHA was analyzed using XPS (Fig. S3 and S4), and the relative proportions of the corresponding functional groups are summarized in Fig. 2c. The C 1 s spectra were deconvoluted into four peaks at 284.3 eV (C=C), 284.8 eV (C–C/C–H), 286.0 eV (C–O), and 288.4 eV (C=O), respectively (Lei et al. 2024; Liu et al. 2024). The introduction of BS was associated with a distinct change in the evolution of carbon surface functionalities. In AHA_{SD}, the carbon structure was predominantly composed of C–C and C–O species. With increasing temperature, the relative content of C–O bonds gradually decreased, while that of C=C bonds first increased and then decreased. These changes which could be associated with the thermal transformation of

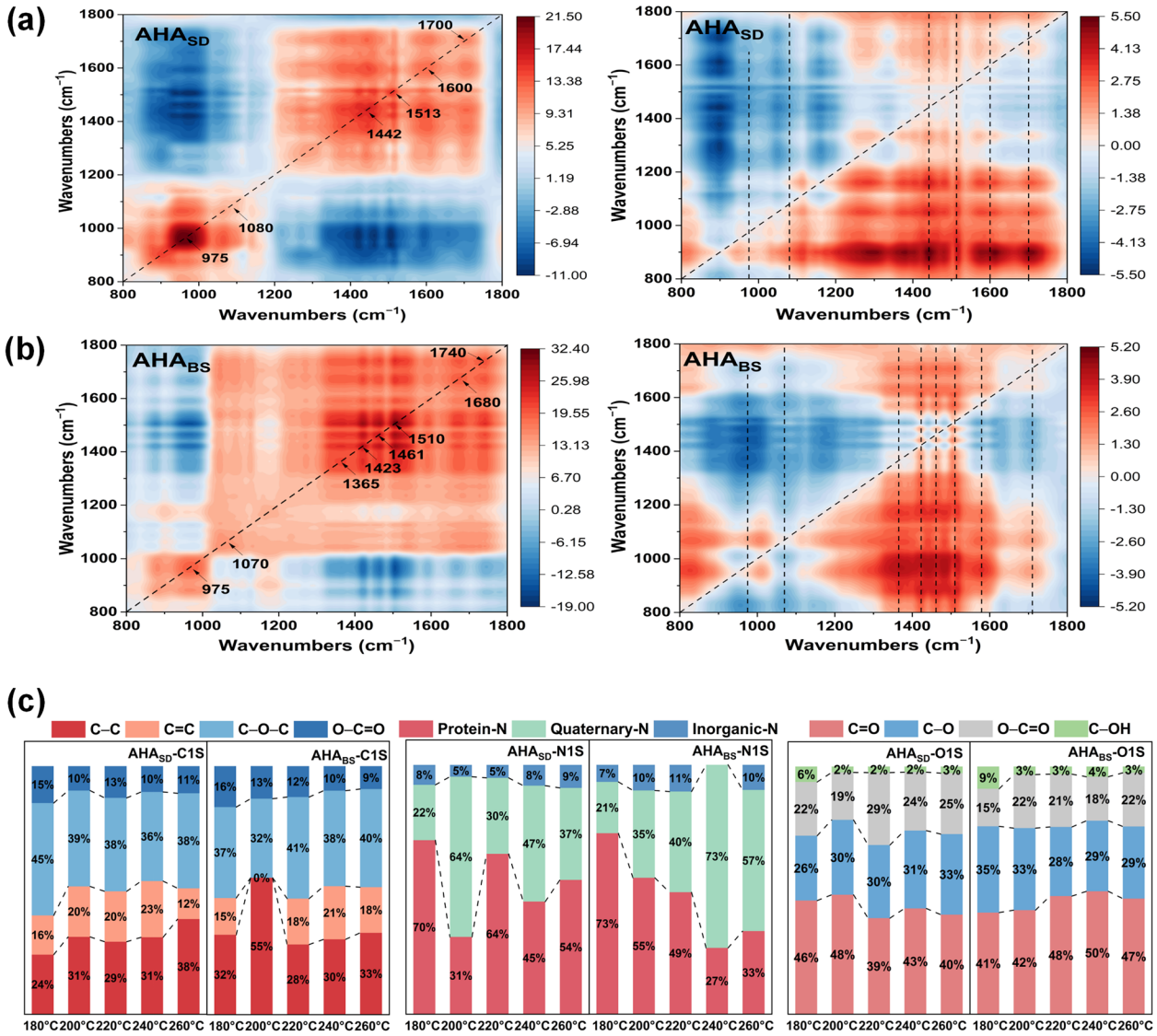


Fig. 2 Surface functional groups of AHA obtained at different temperatures and reaction media: (**a**) and (**b**) synchronous/asynchronous 2D-COS FTIR spectra of AHA_{SD} and AHA_{BS} (800–1800 cm^{-1}); (**c**) XPS spectra (C 1 s, N 1 s, and O 1 s) of AHA

aliphatic and oxygen-containing structures into more aromatic or conjugated C=C structures at lower temperatures, followed by further transformation of cleavage of these structures at higher temperatures (Zhang et al. 2022). Notably, the C=C content in AHA_{BS} reached a minimum at 220 °C and then increased with rising temperature. This trend could reflect the consumption or transformation of C=C-containing precursors, such as trans-olefinic intermediates and lignin-derived monoaromatic compounds, through reactions potentially involving Maillard-type and phenol-amine condensation pathways. These processes could contribute to the formation of nitrogen-containing and more condensed structures, which is consistent with the maximum AHA selectivity obtained at 220 °C.

The N 1 s spectra were fitted with three peaks corresponding to protein-N, quaternary-N, and inorganic-N at 399.9, 401.5, and 402.4 eV, respectively (Wu et al. 2020). In AHA_{SD}, the proportion of protein-N sharply decreased from 70% to 31%, while quaternary-N increased from 22% to 64% as the temperature increased from 180 °C to 200 °C. This suggests a transformation of amine/amide nitrogen toward more condensed or quaternary nitrogen species, potentially involving cyclization or condensation occurring near 200 °C (Wang et al. 2022). Further temperature elevation was accompanied by fluctuations in

quaternary-N content, which could be associated with further structural rearrangement or decomposition of nitrogen-containing species. In AHA_{BS}, the quaternary-N content peaked at 240 °C (73%), suggesting enhanced formation or retention of relatively stable nitrogen-containing structures. This could be related to interactions between nitrogen-containing species and organic acids and other reactive intermediates present in BS, which may favor the formation of more condensed nitrogen-containing structures.

The O 1 s spectra were deconvoluted into four peaks assigned to C=O, C–O, O–C=O, and C–OH groups (Chen et al. 2022; Su et al. 2024). In AHA_{SD}, the C–O content increased from 26% to 33% with rising temperature, suggesting an increased contribution of alcoholic, phenolic, or ether functionalities during the thermal degradation of macromolecular constituents. Unlike the fluctuating C=O pattern in AHA_{SD}, AHA_{BS} exhibited a monotonic increase in C=O content (from 41% to 50%) with temperature, maintaining high levels at elevated temperatures. This trend suggests that the BS environment was associated with greater enrichment or retention of carbonyl-containing structures.

3.3.3 Structural properties

3D-EEM fluorescence spectroscopy was utilized to characterize the humic components of the AHA, as illustrated in Fig. 3a. The fluorescence signals of AHA were primarily distributed in Region III (fulvic-like substances) and Region V (humic-like substances) (Table S5). The intensity of Peak V was markedly higher than that of Peak III, suggesting that AHA contained a greater contribution of humic-like fluorophores, potentially associated with more conjugated structures (Lei et al. 2024; Liu et al. 2025). Fluorescence intensity in both regions generally increased with temperature, with AHA_{SD} exhibiting the highest fluorescence intensity at 240 °C, which could reflect an increased abundance of condensed or conjugated humic-like fluorophores at elevated temperatures. The reaction medium also had a pronounced influence

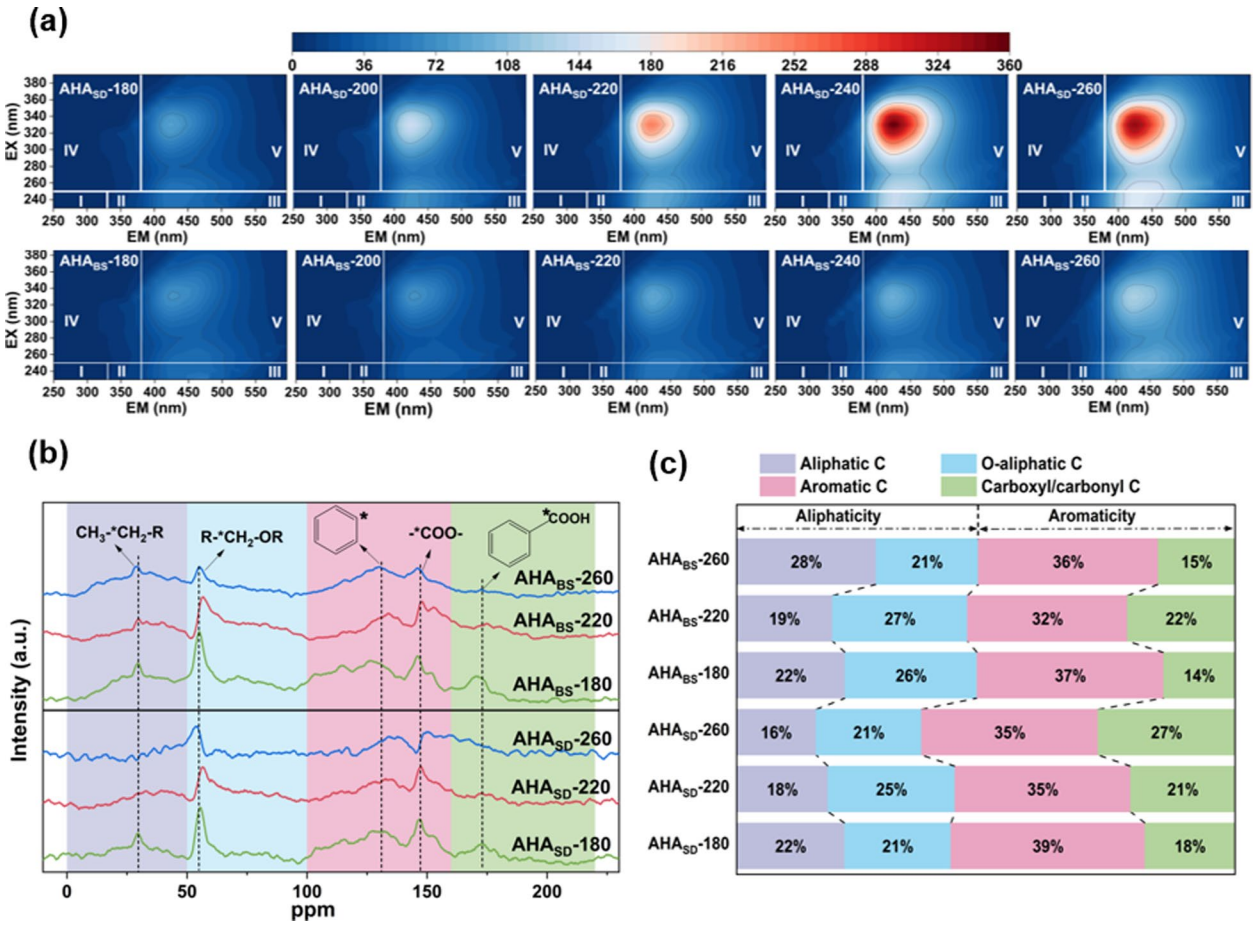


Fig. 3 Structural properties of AHA: **a** 3D-EEM fluorescence spectra; **b** solid-state ^{13}C NMR spectroscopy; and (**c**) relative proportions of carbon functional groups derived from NMR analysis

on the fluorescence characteristics of AHA. The intensity of AHA_{SD} in Region V was markedly higher than that of AHA_{BS}, suggesting a greater abundance of highly fluorescent humic-like structures in AHA_{SD}. In contrast, the lower Region V fluorescence intensity of AHA_{BS}, combined with the presence of amino acids and ammonium ions in BS, could be associated with differences in lignin transformation and a greater contribution of nitrogen-involving reaction pathways, including Maillard-type reactions. These could contribute to the formation of structurally diverse nitrogen-containing humic substances with different fluorescence characteristics. These findings suggest that the reaction medium effectively influences the humification pathway and consequently the structural and optical properties of AHA, providing new opportunities for tuning AHA functionality.

Solid-state ^{13}C NMR spectroscopy was utilized to analyze the carbon skeleton structures of AHA (Fig. 3b) and the relative contents shown in Fig. 3c were estimated from the spectra as a qualitative representation of the major structural groups in AHA. Compared with AHA_{SD}, AHA_{BS} exhibited a higher relative content of aliphatic carbon (0–50 ppm), primarily associated with methyl and methylene carbons. This enrichment could be related to contributions from native lipids, fatty acids, and amino acid side chains present in the BS, some of which could further participate in Maillard-type and condensation reactions during HTH and contribute to the formation of aliphatic N-containing humic substances. This is consistent with the differences observed by 3D-EEM. The pronounced resonance signals observed between 50 and 100 ppm correspond to oxygenated aliphatic carbon, primarily associated with ether (C–O–C) and alcohols/phenolic (C–OH) functionalities (Xu et al. 2025). These could be associated with carbohydrate-derived intermediates and their transformation products. Aromatic carbon (100–160 ppm) represented the dominant component in AHA, suggesting the presence of an aromatic-rich carbon framework. However, the aromatic carbon content exhibited distinct trends between AHA_{SD} and AHA_{BS} with increasing temperature. In AHA_{BS}, the changes in aromatic carbon could reflect contributions from nitrogen-containing aromatic or heterocyclic structures formed through condensation and related reactions. In the carboxyl/carbonyl carbon region (160–220 ppm), AHA_{SD} exhibited higher relative intensities than AHA_{BS}, which could be associated with greater consumption or transformation of carbonyl-containing structures through reactions involving the abundant nitrogen-containing precursors in BS, including Maillard-type pathways. Overall, these results suggest that temperature influences the aromaticity and structural evolution of AHA, while the reaction medium affects the relative contributions of aliphatic, oxygenated, and aromatic carbon structures.

3.3.4 Molecular transformation

The molecular transformation of DOM in AHA under different HTH conditions was characterized using FT-ICR-MS (Fig. 4). Based on the H/C and O/C atomic ratios, the compounds were classified into seven molecular categories (Table S6) (Cai et al. 2023). Under all experimental conditions, the molecular composition was predominantly composed of CHON- and CHO-type compounds, accounting for 36.0–48.3% and 39.8–45.8% of the four elemental groups (CHO, CHON, CHOS, and CHONS), respectively (Fig. 4a). In AHA_{SD}, the relative abundance of CHON compounds decreased from 45.8% to 40.4% with increasing temperature, whereas CHO compounds increased to 48.3%. The relative proportions of lignin-like, lipid, protein/amino sugar, and carbohydrate compounds decreased with increasing temperature, while unsaturated and phenolic compounds increased from 24.3% to 41.9%. This trend suggests that cleavage of ether and C–C bonds in lignin under HTH could generate phenolic monomers and unsaturated acids. Concurrently, hydrolysis and deamination of nitrogenous compounds, lipids, and carbohydrates could generate reactive low-molecular-weight fragments that partially repolymerized into condensed, highly unsaturated aromatic structures. Although the compositional trends in AHA derived from AHA_{BS} were consistent with those in AHA_{SD}, the magnitude of change was greater. The lignin-like fraction decreased by 35.8%, while unsaturated and phenolic compounds substantially increased by 80.9%. This suggests that BS served both as a nitrogen source, contributing to nitrogen incorporation into AHA, and as a mildly alkaline reaction medium that could promote lignin depolymerization into phenolic and aromatic units. Additionally, the DBE_W and AI_{mod} of AHA (Table S7 and Fig. S5) increased with temperature, indicating enhanced unsaturation and aromaticity in the molecular structure.

To elucidate the transformation of DOM during HTH, mass difference network analysis was employed to reveal the relationships between precursors and products (Fig. 4b and 4c). The reactions were categorized into two stages: 180–220 °C (stage I) and 220–260 °C (stage II). In stage I of AHA_{SD}, nitro reduction ($-NO_2+H$, 19.14%) and decarboxylation ($-C_2H_2O_2$, 15.57%) were predominant. Nitro groups could be reduced to amino groups, potentially facilitating subsequent condensation reactions. Concurrently, deoxygenation, decarboxylation ($-CO_2$), dehydration ($-H_2O$), and decarbonylation (–CO), could generate a variety of reactive intermediates bearing carboxylic, carbonyl,

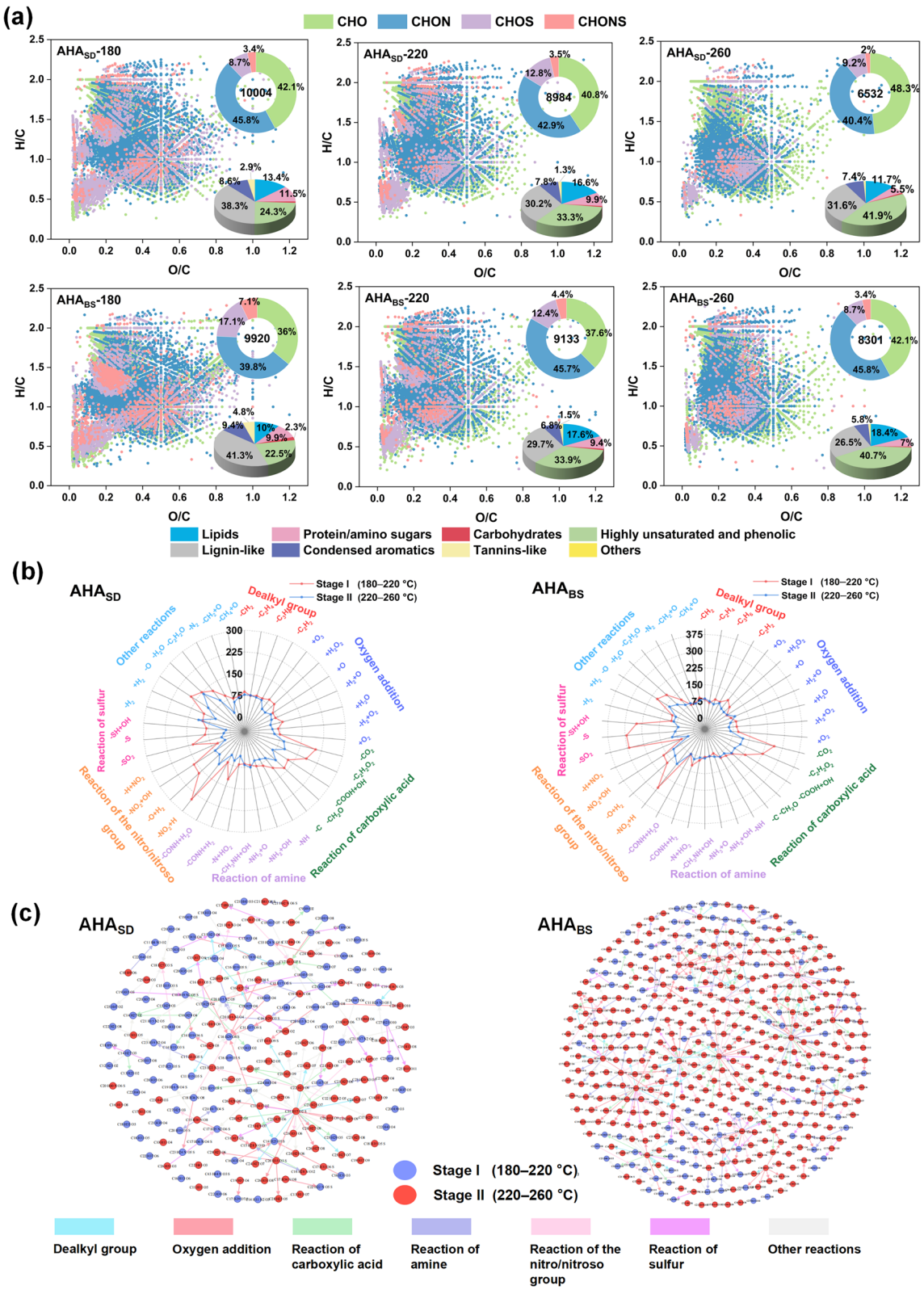


Fig. 4 Molecular transformation of DOM in AHA under different HTH conditions: **a** van Krevelen diagram of molecular composition and relative abundance; **b** radar chart of potential precursor-product pairs under different reaction media; **c** mass difference network of transformation pathways

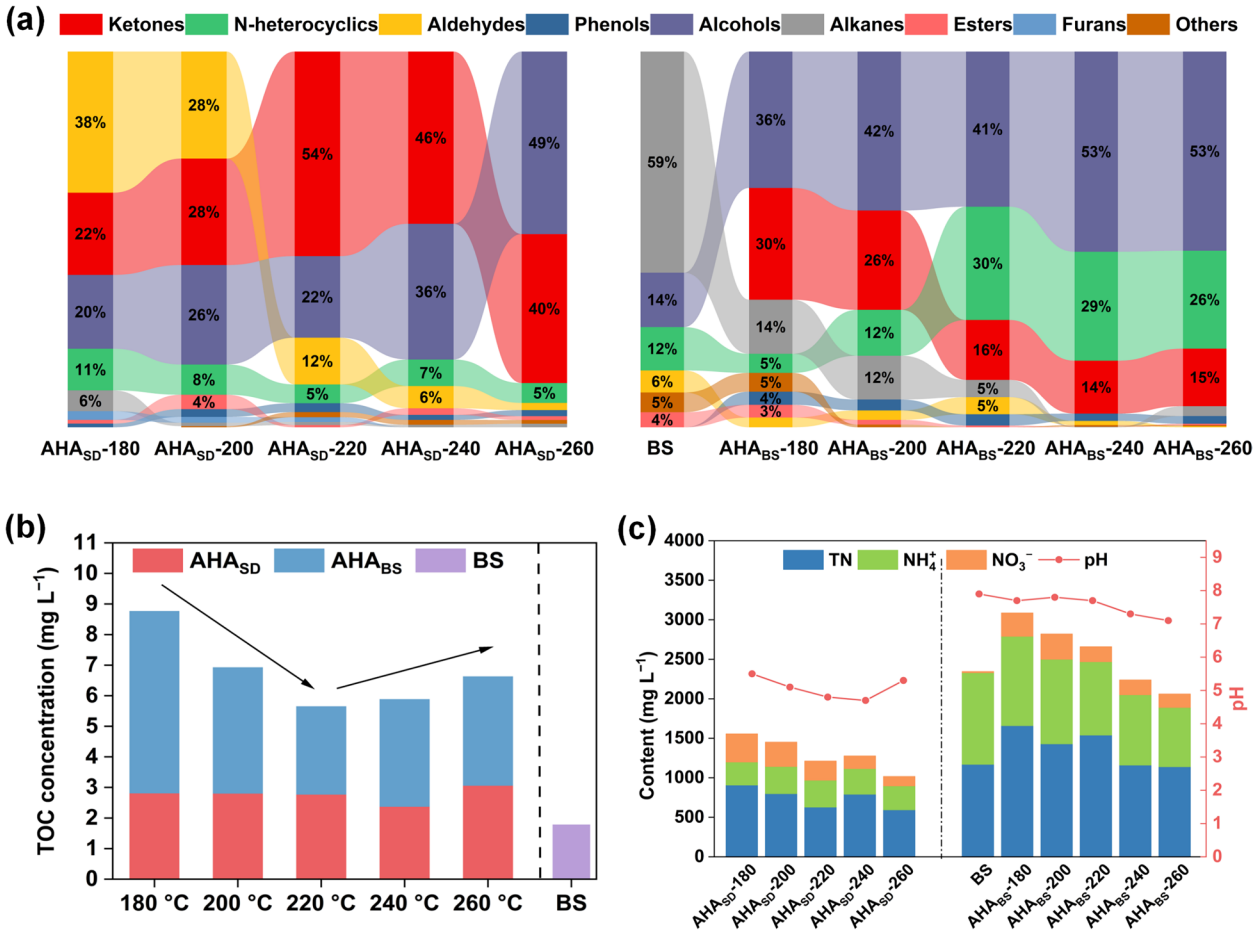


Fig. 5 The composition properties of the aqueous phase: **a** Organic compositions; **b** the content of TOC; **c** the content of NH_4^+, NO_3^-, TN, and pH

and hydroxyl functionalities (Cai et al. 2023). These reactions could promote the formation or amino- and oxygen-bearing precursors that may subsequently undergo condensation to form AHA structure units.

During stage II, the HTH process appeared to be dominated by polymerization and aromatization. The enhanced decarboxylation and deoxygenation could further contribute to the development of aromatic structures and nitrogen incorporation, thereby increasing the degree of unsaturation and aromaticity and favoring the forming of more stable macromolecules structures characteristic of humic substances. As illustrated in Fig. 4c, BS acted as both a reaction medium and a source of diverse molecular precursors, which could broaden the reaction network and increase the complexity of transformation pathways, thereby contributing to greater molecular heterogeneity and chemical diversity of the resulting AHA.

3.4 Aqueous phase properties

3.4.1 Organic compositions

The organic compositions of the aqueous phase obtained under different HTH conditions are presented in Fig. 5a. The detected organic compounds were primarily ketones, phenols, aldehydes, and N-heterocycles, accompanied by minor amounts of alkanes, esters, alcohols, and furans. The composition of the aqueous phase was strongly influenced by both temperature and reaction medium. In the system using deionized water as the reaction medium, increasing the temperature from 180 °C to 220 °C was associated with enhanced degradation and depolymerization of macromolecular structures (e.g., carbohydrates and lignin), as evidenced by the increased relative abundance of ketones and phenols. Meanwhile, aldehyde concentrations decreased significantly, likely due to their participation as reactive intermediates in condensation reactions with the generated phenolic compounds, potentially forming larger aromatic precursors. The introduction of nitrogen-rich BS substantially altered the hydrothermal humification pathway. As the temperature

increased, the relative contents of alkanes and ketones decreased, accompanied by a pronounced increase in phenols and nitrogen-containing heterocycles. The transformation of alkanes and lignin-derived compounds may generate ketone-containing intermediates, which could subsequently react with nitrogen-containing compounds in BS to form nitrogen-containing heterocycles. With further temperature increase, phenolic compounds accumulated, possible due in part to the high structural stability of their aromatic rings. Meanwhile, a portion of the nitrogen-containing heterocycles could undergo further condensation and become incorporated into larger molecular frameworks, potentially contributing to the formation of nitrogen-enriched aromatic AHA.

3.4.2 The total carbon content

Figure 5b presents the total organic carbon (TOC) content in the aqueous phase. The TOC concentration exhibited a pattern of initially decreasing and then increasing as temperature rose. The variation was more pronounced in the BS system. In the 180–220 °C range, nitrogen-containing substances in BS could participate in Maillard reactions with aldehydes produced from carbohydrate degradation, thereby consuming dissolved carbon and favoring the formation and separation of insoluble polymers from the aqueous phase. At higher temperatures, the cleavage of strong chemical bonds in macromolecules such as lignin and humic acids could generate soluble phenolic compounds and other derivatives that were released into the aqueous phase, leading to a subsequent increase in TOC. These trends are consistent with the observed changes in organic components.

3.4.3 The nitrogen content and pH

Figure 5c illustrates the variations in nitrogen content and pH in the aqueous phase. The concentrations of TN, NH_4^+–N, and NO_3^-–N in BS were 1170, 1160, and 14.1 mg L^{-1}, respectively. Owing to the high nitrogen content in BS, the AHA_{BS} system exhibited markedly higher nitrogen content and pH in the aqueous phase compared with AHA_{SD}. The decrease in TN concentration could be associated with Maillard reactions between reducing sugars (generated through carbohydrate hydrolysis in SD) and amino compounds, as well as condensation and polymerization of nitrogenous intermediates. These reactions could consume substantial amounts of soluble nitrogen species in the aqueous phase and contribute to their incorporation into solid-phase humic substances ultimately resulting in a decrease in TN concentration. An inflection point occurred at 240 °C, which could be associated with enhanced hydrolysis. In contrast, the inflection points for AHA_{BS} shifted to a lower temperature of 220 °C, accompanied by a sharp 74.12% reduction in NH_4^+–N concentration. This shift could be attributed to the abundant nitrogen sources in BS (e.g., amino acids and ammonium salts), which not only supplied precursors but also provided an alkaline environment that could facilitate SD decomposition at lower temperatures. This combined effect could promote Maillard and condensation-polymerization reactions among intermediates, thereby contributing to greater nitrogen incorporation into AHA.

3.5 Possible reaction mechanisms

Figure 6 presents two distinct reaction pathways for the hydrothermal synthesis of AHA from SD under different reaction media. In the deionized water system, lignin and carbohydrates have been identified as critical precursors for constructing the structural framework of AHA (Shao et al. 2023a, b). As the temperature increased, phenolic and carboxyl groups derived from lignin decomposition, along with their derivatives, could undergo rearrangement, condensation, and aromatization to form the core skeleton of AHA (Liu et al. 2024). Meanwhile, carbohydrates (cellulose and hemicellulose) could rapidly degrade to produce key intermediates such as furans, aldehydes, and a variety of aliphatic–aromatic compounds. These intermediates could either be incorporated into the AHA backbone through condensation and aromatization reactions or be attached as reactive side chains, ultimately contributing to the formation of AHA enriched with aromatic units, aliphatic components, and diverse functional groups.

When BS was used as the reaction medium, it acted as a reactive nitrogen source that not only could enhance the degradation of SD but also supplied essential nutrients for AHA synthesis. The alkaline conditions of BS could facilitate lignin decomposition by cleaving C–O–C linkages within lignin and ether/ester bonds in lignin-carbohydrate complexes, releasing essential precursors for humification (Nagel and Zhang 2019). Simultaneously, the alkaline environment might promote the oxidation of lignin-derived phenolic structures and decarboxylation of carboxyl groups (–COOH) (Wang et al. 2019), providing a favorable basis for the formation of humic-like macromolecules. Nitrogen and other reactive species in BS could further participate in amidation and amine-aldehyde condensation reactions to produce nitrogen-enriched precursors, which would subsequently undergo dehydrative cyclization to form aromatic structures, such as benzene and naphthalene rings, at elevated temperatures (Song et al. 2025). Simultaneously, Maillard reactions between reducing sugars (e.g., glucose) and amines could further promote AHA formation. Through this process, nitrogen could be incorporated into stable heterocyclic structures through C–N covalent bonding

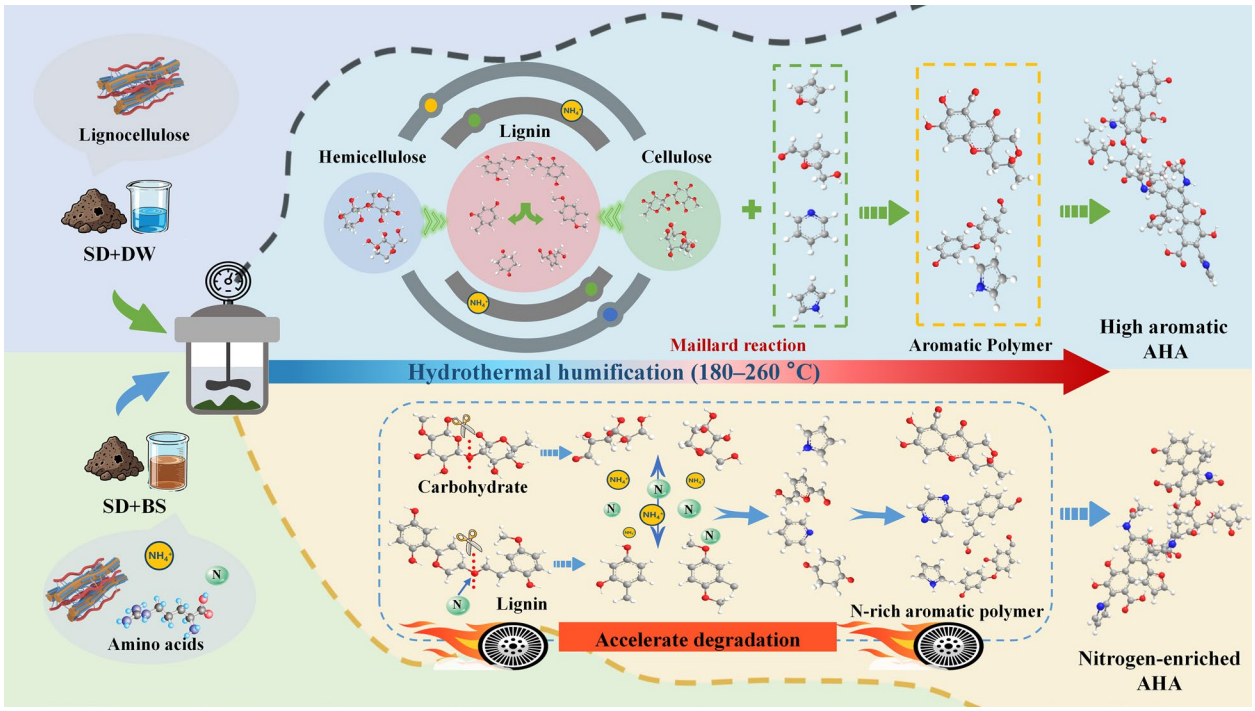


Fig. 6 Proposed reaction pathways for AHA formation under different temperatures and reaction medium

and retained within the AHA matrix (Jiang et al. 2022), which is consistent with the XPS results.

Collectively, these possible synergistic mechanisms could facilitate the formation of structurally stable and nutrient-enriched AHA macromolecules. Overall, both the reaction temperature and reaction medium strongly influenced the synthesis pathway and characteristics of AHA. Higher temperatures could accelerate the release and reactivity of intermediates, enhance condensation and polymerization reactions, and thereby increase AHA selectivity. However, excessively high temperatures may induce severe dehydration and decarboxylation, leading to undesired humin formation. The reaction medium further regulated cross-linking and aromatization pathways. BS not only facilitated SD hydrolysis to generate more intermediates but also contributed nitrogen to the evolving AHA structure, thereby potentially enhancing the chemical diversity, structural complexity, and application potential of the resulting AHA.

4 Conclusions

This study demonstrates that HTH can effectively convert BD into nitrogen-enriched AHA, with reaction temperature and medium strongly influencing nitrogen fixation and reaction pathways. Lignin degradation products could undergo rearrangement, polycondensation, and aromatization to form an aromatic-rich AHA core structure in the deionized water system. The highest AHA selectivity (40.16%) was obtained at 220 °C when BS was used as the medium. The presence of BS likely served multiple roles as a nitrogen source, alkaline reaction medium, and potential reaction accelerator, providing reactive precursors for Maillard and amine-aldehyde condensation reactions. Meanwhile, its alkaline environment may have facilitated lignin depolymerization and intermediate formation, thereby contributing to nitrogen incorporation into stable heterocyclic structures. These combined effects could enhance the reactivity of BD and increase molecular diversity ultimately yielding structurally stable, nutrient-rich AHA. These insights expand the value-added utilization of BD and offer a promising strategy for producing nitrogen-enriched humic materials for soil amendment applications. Notably, this study focused on the chemical characterization and structural analysis of AHA, while its agronomic performance, environmental safety, nutrient-release behavior, and phytotoxicity were not experimentally evaluated. Therefore, further studies, including plant-growth assays, soil incubation experiments, and ecotoxicological assessments, are warranted to confirm its practical applicability and environmental compatibility.

Supplementary Information

The online version contains supplementary material available at https://doi.org/10.1007/s42773-026-00662-4.

Supplementary material 1

Author contributions

Yanan Zhao: Writing–original draft, conceptualization, formal analysis, methodology, and investigation. Ziyun Liu: Methodology, formal analysis, and writing–review & editing. Zonglu Yao: Methodology, conceptualization, and supervision. Dan Wang: Formal analysis, writing–review & editing. Jinting Su: Writing–review & editing. Jihua Yang: Supervision and data collection. Lili Huo: Writing–review & editing. Jixiu Jia: Writing–review & editing. Hugang Li: Writing–review & editing. Lixin Zhao: Project administration and funding acquisition. All authors read and approved the final manuscript.

Funding

This work was supported by Innovation Program of Chinese Academy of Agricultural Sciences (CAAS-CSGLCA-202401), The Agricultural Science and Technology Innovation Program (ASTIP), and National Natural Science Foundation of China (No. 32301726).

Data availability

The datasets used or analyzed during the current study are available from the corresponding author upon reasonable request.

Declarations

Competing interests

Zonglu Yao is an EBM of the journal Biochar, and he was not involved in the peer-review or handling of the manuscript. The authors have no competing interests to declare that are relevant to the content of this article.

Author details

[1]Institute of Environment and Sustainable Development in Agriculture, Chinese Academy of Agricultural Sciences, Beijing 10081, China. [2]Key Laboratory of Low-carbon Green Agriculture in North China, Ministry of Agriculture and Rural Affairs P. R. China, Beijing, China. [3]College of Agronomy and Biotechnology/Center of Biomass Engineering, China Agricultural University, Beijing 100193, China. [4]College of Environment and Ecology, Taiyuan University of Technology, Taiyuan 030600, China.

Received: 26 November 2025 Revised: 14 September 2026 Accepted: 30 September 2026
Published online: 23 October 2026

References

Ahmad F, Silva EL, Varesche MBA (2018) Hydrothermal processing of biomass for anaerobic digestion – a review. Renew Sustain Energy Rev 98:108–124. https://doi.org/10.1016/j.rser.2018.09.008

Basar IA, Liu H, Carrere H et al (2021) A review on key design and operational parameters to optimize and develop hydrothermal liquefaction of biomass for biorefinery applications. Green Chem 23:1404–1446. https://doi.org/10.1039/d0gc04092d

Cai S, Zhang Y, Hu A et al (2023) Dissolved organic matter transformation mechanisms and process optimization of wastewater sludge hydrothermal humification treatment for producing plant biostimulants. Water Res 235:119910. https://doi.org/10.1016/j.watres.2023.119910

Cao Z, Jung D, Olszewski MP et al (2019) Hydrothermal carbonization of biogas digestate: effect of digestate origin and process conditions. Waste Manag 100:138–150. https://doi.org/10.1016/j.wasman.2019.09.009

Celletti S, Bergamo A, Benedetti V et al (2021) Phytotoxicity of hydrochars obtained by hydrothermal carbonization of manure-based digestate. J Environ Manage 280:111635. https://doi.org/10.1016/j.jenvman.2020.111635

Chen P, Yang R, Pei Y et al (2022) Hydrothermal synthesis of similar mineral-sourced humic acid from food waste and the role of protein. Sci Total Environ 828:154440. https://doi.org/10.1016/j.scitotenv.2022.154440

Daer D, Luo L, Shang Y et al (2024) Co-hydrothermal carbonization of waste biomass and phosphate rock: promoted carbon sequestration and enhanced phosphorus bioavailability. Biochar 6:70. https://doi.org/10.1007/s42773-024-00356-9

Deng F, Cao Z, Luo Y et al (2023) Production of artificial humic acid from corn straw acid hydrolysis residue with biogas slurry impregnation for fertilizer application. J Environ Manage 345:118845. https://doi.org/10.1016/j.jenvman.2023.118845

Devi P, Eskicioglu C (2024) Effects of biochar on anaerobic digestion: a review. Environ Chem Lett 22:2845–2886. https://doi.org/10.1007/s10311-024-01766-8

Fan Y, Hornung U, Dahmen N et al (2018) Hydrothermal liquefaction of protein-containing biomass: study of model compounds for Maillard reactions. Biomass Convers Biorefin 8:909–923. https://doi.org/10.1007/s13399-018-0340-8

Gao J, Li L, Yuan S et al (2022) The neglected effects of polysaccharide transformation on sludge humification during anaerobic digestion with thermal hydrolysis pretreatment. Water Res 226:119249. https://doi.org/10.1016/j.watres.2022.119249

Guo X, Liu H, Wu S (2019) Humic substances developed during organic waste composting: formation mechanisms, structural properties, and agronomic functions. Sci Total Environ 662:501–510. https://doi.org/10.1016/j.scitotenv.2019.01.137

MHB Hayes RS Swift (2020) Vindication of Humic Substances as a Key Component of Organic Matter in Soil and Water https://doi.org/10.1016/bs.agron.2020.05.001

Hu J, Liu C, Zhang W et al (2025) Decomposing the molecular complexity and transformation of dissolved organic matter for innovative anaerobic bioprocessing. Nat Commun. https://doi.org/10.1038/s41467-025-60240-3

Jiang H, Deng F, Luo Y et al (2022) Hydrothermal carbonization of corn straw in biogas slurry. J Clean Prod 353:131682. https://doi.org/10.1016/j.jclepro.2022.131682

Ke L, Liu X, Du B et al (2022) Component analysis and risk assessment of biogas slurry from biogas plants. Chin J Chem Eng 44:182–191. https://doi.org/10.1016/j.cjche.2021.05.039

Kim J, Oh J, Tsang YF et al (2020) CO2-assisted catalytic pyrolysis of digestate with steel slag. Energy (Oxf) 191:116529. https://doi.org/10.1016/j.energy.2019.116529

Lehmann J, Bossio DA, Kogel-Knabner I et al (2020) The concept and future prospects of soil health. Nat Rev Earth Environ 1:544–553. https://doi.org/10.1038/s43017-020-0080-8

Lei T, Su J, Chang L et al (2024) Artificial humic acid produced from wet distillers grains in a microwave-assisted hydrothermal process: physicochemical characteristics and stimulation to plant growth. Chemosphere 364:142979. https://doi.org/10.1016/j.chemosphere.2024.142979

Li C, Cai R (2022) Preparation of solid organic fertilizer by co-hydrothermal carbonization of peanut residue and corn cob: a study on nutrient conversion. Sci Total Environ 838:155867. https://doi.org/10.1016/j.scitotenv.2022.155867

Liu T, Zhou X, Li Z et al (2019) Effects of liquid digestate pretreatment on biogas production for anaerobic digestion of wheat straw. Bioresour Technol 280:345–351. https://doi.org/10.1016/j.biortech.2019.01.147

Liu Z, Su J, Yao Z et al (2024) Enhancing humic acids production from cornstalk under fast hydrothermal conditions: insights into new pathways of skeleton self-polymerization and branch growth. Bioresour Technol 406:131020. https://doi.org/10.1016/j.biortech.2024.131020

Liu W, Xia R, Li G et al (2025) Three-dimensional analysis of foulant distribution in ultrafiltration membrane treating biogas slurry. J Membr Sci 735:124571. https://doi.org/10.1016/j.memsci.2025.124571

Lu J, Cheng M, Zhao C et al (2022) Application of lignin in preparation of slow-release fertilizer: current status and future perspectives. Ind Crops Prod 176:114267. https://doi.org/10.1016/j.indcrop.2021.114267

Marzban N, Libra JA, Rotter VS et al (2024) Maximizing the value of liquid products and minimizing carbon loss in hydrothermal processing of biomass: an evolution from carbonization to humification. Biochar 6:44. https://doi.org/10.1007/s42773-024-00334-1

Mikusińska J, Szkadłubowicz K, Prus Z et al (2025) Fuel properties characterization of hydrochars derived from agricultural digestate. Renew Energy 244:122639. https://doi.org/10.1016/j.renene.2025.122639
Nagel E, Zhang C (2019) Hydrothermal decomposition of a lignin dimer under neutral and basic conditions: a mechanism study. Ind Eng Chem Res 58:18866–18880. https://doi.org/10.1021/acs.iecr.9b00400
Shao Y, Bao M, Huo W et al (2023a) From biomass to humic acid: is there an accelerated way to go? Chem Eng J 452:139172. https://doi.org/10.1016/j.cej.2022.139172
Shao Y, Huo W, Ye R et al (2023b) Hydrothermal humification of lignocellulosic components: who is doing what? Chem Eng J 457:141180. https://doi.org/10.1016/j.cej.2022.141180
Song S, Zhang T, Shi Z et al (2025) Biogas slurry impregnation-driven hydrothermal synthesis of artificial humic acid: mechanistic insights and agricultural implications. Bioresour Technol 439:133279. https://doi.org/10.1016/j.biortech.2025.133279
Su X, Zhang R, Cao H et al (2024) Adsorption of humic acid from different organic solid waste compost to phenanthrene, is fluorescence excitation or quenching? Environ Pollut 347:123712. https://doi.org/10.1016/j.envpol.2024.123712
Wang R, Zhou B, Wang Z (2019) Study on the preparation and application of lignin-derived polycarboxylic acids. J Chem. https://doi.org/10.1155/2019/5493745
Wang R, Lin Z, Meng S et al (2022) Effect of lignocellulosic components on the hydrothermal carbonization reaction pathway and product properties of protein. Energy (Oxf) 259:125063. https://doi.org/10.1016/j.energy.2022.125063
Wang X, Zhang D, Wang F et al (2024) Effects of biogas slurry on hydrothermal carbonization of digestate: synergistic valorization of hydrochars and aqueous phase. J Environ Manage 362:121317. https://doi.org/10.1016/j.jenvman.2024.121317
Wang D, Liu Z, Su J et al (2025) Mechanistic insights into nitrogen-mediated carbon transformation during hydrothermal humification for the synthesis of nutrient-enriched artificial humic acids. Bioresour Technol 437:133100. https://doi.org/10.1016/j.biortech.2025.133100
Wu B, Berg SM, Remucal CK et al (2020) Evolution of N-containing compounds during hydrothermal liquefaction of sewage sludge. ACS Sustain Chem Eng 8:18303–18313. https://doi.org/10.1021/acssuschemeng.0c07060
Xu Z, Song H, Zhang S et al (2019) Co-hydrothermal carbonization of digested sewage sludge and cow dung biogas residue: investigation of the reaction characteristics. Energy (Oxf) 187:115972. https://doi.org/10.1016/j.energy.2019.115972
Xu M, Chen P, Wang J et al (2025) Oxygen-promoted low-temperature hydrothermal conversion of Chinese medicinal herbal residues into humic acids. Carbon Neutr. https://doi.org/10.1007/s43979-025-00127-w
Zhang D, Wang F, Shen X et al (2018) Comparison study on fuel properties of hydrochars produced from corn stalk and corn stalk digestate. Energy (Oxf) 165:527–536. https://doi.org/10.1016/j.energy.2018.09.174
Zhang C, Wang X, Shao M et al (2022) Synthesis of nitrogen-enriched hydrochar via co-hydrothermal reaction of liquid digestate and corn stalk. Sci Total Environ 836:155572. https://doi.org/10.1016/j.scitotenv.2022.155572
Zhou X, Li J, Zhang J et al (2022) Bioaugmentation mechanism on humic acid formation during composting of food waste. Sci Total Environ 830:154783. https://doi.org/10.1016/j.scitotenv.2022.154783
Zhu Y, Cao Y, Fu B et al (2024) Waste milk humification product can be used as a slow release nano-fertilizer. Nat Commun 15:128. https://doi.org/10.1038/s41467-023-44422-5